Effect of Hot-rolling Deformation on Microstructure and Mechanical Properties of Nd$_2$Fe$_{14}$B$_p$/Al-5Co-0.4Sm Composites

Huang Jun-jie [iD], Huang You-wei [iD], He Jia-xin [iD], Kang Ma [iD] and Wang Hong-ming [iD]*

School of Materials Science & Engineering, Jiangsu University, Zhenjiang, Jiangsu Province 212013, PR China

ARTICLE INFO

ABSTRACT

Nd$_2$Fe$_{14}$B$_p$/Al-5Co-0.4Sm composites were prepared via microwave sintering and hot rolling. The effects of hot-rolling deformation on the microstructure and mechanical properties of Nd$_2$Fe$_{14}$B$_p$/Al-5Co-0.4Sm composites were studied. The results showed that the internal porosity of the composites significantly decreased when the hot-rolling deformation rate was 45%. The Nd$_2$Fe$_{14}$B particles were broken into fine particles under rolling stress. Consequently, the particles were uniformly distributed. Moreover, numerous high-density dislocations were observed around the particles, which improved the strength and toughness of the material. When the deformation rate was 45%, the micro-nano hardness and elastic modulus of the interface of the composites were 3.6 and 91 GPa, respectively. The interfacial deformation resistance of the composites was significantly higher than that of the composites before rolling. The tensile strength of Nd$_2$Fe$_{14}$B$_p$/Al-5Co-0.4Sm composites increased as the deformation rate increased, whereas the elongation gradually decreased. Furthermore, when the deformation rate was 45%, the tensile strength and elongation of the composites were 161 MPa and 6.5%, respectively. The tensile strength was 14.2% higher than that of the unrolled sample.

*Corresponding Author
Email: ujswang@sina.com
Tel: +(86) 13921595660

1. Introduction

The development of lightweight automobiles is one of the most effective measures to save energy and reduce emissions. At present, automobile weight can be reduced by replacing traditional steel structural materials with aluminum steel and carbon fiber composite structural materials. However, the weight reduction of the magnetic materials has not been reported. The traditional magnetic materials mainly contain iron. For example, $Nd_2Fe_{14}B$ has a density of 7.5 g/m^3, which is not conducive to lightweight automobiles. In addition, $Nd_2Fe_{14}B$ is brittle and has fracture toughness similar to ceramics [1, 2]. Particle-reinforced aluminum matrix composites have favorable properties, including low density, high specific strength, high specific modulus, outstanding wear resistance, and good electrical and thermal conductivities [3-6]. As a result, they are widely used in aviation, aerospace, automotive, electronic devices, and other fields. In the study, to reduce the density and brittleness of existing magnetic materials, $Nd_2Fe_{14}B$ particle-reinforced aluminum matrix composites were prepared. The composites are expected to exhibit excellent magnetic properties and good plastic toughness.

In previous work, powder metallurgy and microwave sintering were used to prepare $Nd_2Fe_{14}B_p$/Al and $Nd_2Fe_{14}B_p$/Al-Co composites [7, 8]. Microwave sintering achieved rapid sintering at relatively low temperatures, reduced the interface reaction between matrix and reinforced particles, and prevented the excessive growth of crystal grains [9-15]. The Sm element was added to the composites to regulate the properties of $Nd_2Fe_{14}B_p$/Al-Co composites. Sm interacted with Al at the interface between Al and $Nd_2Fe_{14}B$ to form Al_3Sm, which improved the bonding strength between Al and $Nd_2Fe_{14}B$ particles and strengthened the interface. However, the porosity and the particle segregation in the composites could not be eliminated. To further improve the microstructure and comprehensive properties, secondary processing methods, such as rolling, forging, and hot extrusion, are usually adopted. Among them, the rolling method can efficiently control the deformation rate of materials. Therefore, in this study, the effects of the hot-rolling deformation rate on the microstructure and properties of $Nd_2Fe_{14}B_p$/Al-5Co-0.4Sm composites were investigated.

The effects of rolling on the microstructure and mechanical properties of particle-reinforced aluminum matrix composites have attracted considerable scholarly attention, and the related mechanisms have been explored [16]. El-Sabbagh studied the hot-rolling behavior of stirred cast SiC particle-reinforced Al6061 and Al6082 composites and found that as the deformation rate increased, the porosity linearly decreased, and the particle agglomeration significantly decreased [17-19]. Feng prepared the SiC_p/2024Al composite sheets through the stirring casting-hot extrusion-rolling process and found that the failure mechanism of the material mainly changed from SiC particle pullout to SiC particle fracture. The finding also revealed that the high temperature deformation improved the interface bonding between the reinforcement particles and the base alloy [20]. Chen conducted rolling research on the forged W_p/2024 composite blank. Previous studies found that the forged W_p/2024Al composite materials had a change process of densification, loosening, re-densification, and stabilization during the rolling process. Ran investigated hot-rolled in situ ZrB_2 nanoparticle-reinforced AA6111 composites and found that the particle clusters uniformly distributed and then agglomerated [21].

This study aimed to improve the mechanical properties of $Nd_2Fe_{14}B_p$/Al-5Co-0.4Sm composites using the hot-rolling method. Modern testing technologies were used to investigate the mechanisms of deformation rate on microstructure and mechanical properties. The study will provide valuable information for the research on the hot-rolling secondary processing of advanced metal matrix composites with excellent magnetic and mechanical properties.

2. Experimental

2.1. Materials

The raw materials used in this work were commercial powders of Al, Co, Sm, and $Nd_2Fe_{14}B$. The particle size of aluminum powder was 10 μm. The particle sizes of $Nd_2Fe_{14}B$, Co, and Sm were 45 μm. The purities of these powders were 99.9%. The $Nd_2Fe_{14}B$ was bonded $Nd_2Fe_{14}B$ powder prepared using a rapid quenching method.

The powder was ball-milled using a planetary ball mill in stages. First, $Nd_2Fe_{14}B$ powder was ball-milled. Then, all the powders were mixed using ball milling according to the proportion in Table **1**. The ball milling medium was a zirconia ball (diameters were 5, 10, and 15 mm with adding ratio of 4:2:1), and the ratio of the ball to the material was 5:1. Absolute ethanol was used as a control agent in the ball milling process. The milling speed of $Nd_2Fe_{14}B$ single ball milling was 200 r/min, and the milling time was 12 h. The ball milling speed for the mixing process was 120 r/min with a ball milling time of 8 h. After each stage of ball milling, anhydrous ethanol was evaporated using the vacuum drying box.

Table 1:   Component of composites.

Powder Types	Mass Ratio/wt%
$Nd_2Fe_{14}B_p$/Al-5Co-0.4Sm	Al: 74.6; $Nd_2Fe_{14}B$: 20.0; Co: 5.0; Sm0.4

The dehydrated powder was transferred into a rubber mold, and two strong magnets were placed at the top and bottom of the mold. Then, the mold was placed in a cold isostatic pressing device at a constant pressure of 300 MPa for 3min. The reason for placing two strong magnets was to make the magnetic powder obtain a preliminary magnetic orientation.

Samples obtained by magnetic isostatic pressing were sintered in a vacuum microwave sintering furnace (WBMW-JS2) at a heating rate of 30℃/min and a temperature of 580℃ for 30 min to obtain high-compactness bulk $Nd_2Fe_{14}B_p$/Al-5Co-0.4Sm composites.

2.2. Hot-rolling Process

The sintered composite materials were cut into 60 mm × 30 mm × 12 mm rectangular rolling samples using wire cutting, and the edges and corners were polished. This experiment was conducted using a heated asynchronous rolling mill with a rolling force of 14000 N and a speed of 6 m/min. Before the rolling process, the samples of $Nd_2Fe_{14}B_p$/Al-5Co-0.4Sm composites were placed in a furnace and heated to 480℃ at a rate of 400℃/h. The holding time of samples in the heating furnace at 480℃ was 30 min. In addition, the mill was heated to 100℃ before rolling. The designed deformation rates of samples were 15, 30, 45, and 60%.

2.3. Testing Approach

Scanning electron microscope (SEM, S-3400 N) combined with the energy dispersive spectrometer (EDS, FEI NovaNano450) and the transmission electron microscope (TEM, JEM-2100, Tecnai-G2) were used to characterize the morphology, crystal grain, structure, and tensile fracture. The electronic universal testing machine (D2-200-N) was used for tensile experiments. The size of the tensile sample is shown in Fig. (**1**). The nanoindentation hardness tester (TTX-NHT3) was used to analyze the micro-nano mechanical properties of the matrix, reinforcement, and interface of the composites. The loading pressure was set to 10 mN, the loading and unloading rates were set to 20 mN/min, and the holding time was 10 s.
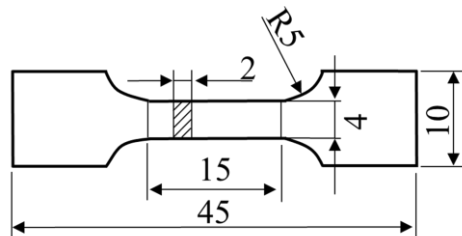

Figure 1: Dimension of the tensile specimen (mm).

3. Results and Discussion

3.1. Microstructure of Sintered Composites

Fig. (**2**) shows the SEM images of the microwave-sintered $Nd_2Fe_{14}B_p$/Al-5Co-0.4-Sm composites. Pores were observed in $Nd_2Fe_{14}B_p$/Al-5Co-0.4Sm composites before hot rolling. The $Nd_2Fe_{14}B$ particles were large and unevenly distributed in the matrix, and the non-particle area was large. Agglomerations of $Nd_2Fe_{14}B$ particles were observed in some areas (as shown in mark 1). Co particles were distributed at the grain boundaries of the aluminum matrix, with a certain agglomeration.
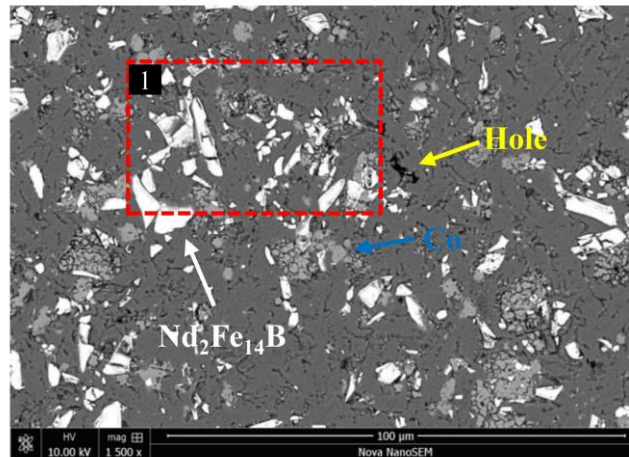
Figure 2: SEM images of the microwave-sintered $Nd_2Fe_{14}B_p$/Al-5Co-0.4Sm composites.

Fig. (**3**) shows the SEM images of hot-rolled $Nd_2Fe_{14}B_p$/Al-5Co-0.4Sm with different deformation rates (15, 30, 45, and 60%). As shown in Fig. (**3a**), when the deformation rate of the $Nd_2Fe_{14}B_p$/Al-5Co-0.4Sm composites was 15%, the distribution, size, and morphology of the $Nd_2Fe_{14}B$ particles underwent some changes. The $Nd_2Fe_{14}B$ particles were elongated along the rolling direction and some clusters were retained, but the particle free area was still large.

When the deformation rate was 30%, the uniformity of the distribution of $Nd_2Fe_{14}B$-reinforced particles gradually increased (Fig. **3b**), and the agglomeration of the particle decreased. As the deformation rate increased, the aluminum matrix deformed. Owing to the high strength of $Nd_2Fe_{14}B$ particles, the existing pressure could not cause significant deformations of the $Nd_2Fe_{14}B$ particles. To adapt to the deformation of the aluminum matrix, the $Nd_2Fe_{14}B$ particles flowed and rotated during the rolling process, which dispersed the originally agglomerated $Nd_2Fe_{14}B$-enhanced particles and gradually reduced the cluster size. Finally, the $Nd_2Fe_{14}B$-reinforcing particles were more evenly distributed in the aluminum matrix, which was beneficial to exert the pinning strengthening effect of the $Nd_2Fe_{14}B$-reinforcing particles, thus significantly improving the performance of the composites.

As shown in Fig. (**3c**), when the hot-rolling deformation was 45%, defects such as internal pores in the composites were significantly reduced. The brittle $Nd_2Fe_{14}B$ particles were broken into fine particles under the action of rolling stress, and the overall uniformity of distribution was improved, thus reducing particle agglomeration. As shown in Fig. (**3d**), when the rolling deformation was 60%, the grains were further refined with the increase in the rolling deformation. However, the internal stress of the material increased due to excessive deformation, which led to fine pore defects between the reinforced phase and the matrix. Because different materials have different bearing capacities, the breakage of $Nd_2Fe_{14}B$ particles will lead to an uncoordinated collision and torsion in the deformation process, resulting in void defects.

When the thickness reduction percentage changed along 15%→30%→45%, the grains of the aluminum matrix were gradually elongated and significantly oriented. The matrix grains were banded, and the width of the banded grains became relatively narrow. This phenomenon was because, during the rolling process of the composite

materials, the edge of the sample was subjected to the compressive stress of the roller, and the central area of the sample was subjected to the outward extrusion stress. At a deformation rate of 60%, dynamic recrystallization occurred, and local grains grew. This phenomenon was because the hot rolling was performed at a temperature higher than the recrystallization temperature of composites. When the deformation was lower than the critical deformation of recrystallization, only dynamic recovery occurred without dynamic recrystallization. Conversely, when the deformation was higher than the critical deformation, complete recrystallization occurred, and partial recrystallization occurred between the composites [22-25].

When the deformation rate changed along 15%→30%→45%, the porosity of the composites gradually decreased, and the compactness increased. When the deformation rate increased to 60%, the interfacial bonding ability between $Nd_2Fe_{14}B$ particles and the matrix worsened due to the crushing of many $Nd_2Fe_{14}B$ particles; consequently, many holes appeared, decreasing compactness.

SEM microstructure analysis revealed that the rolling deformation rate of 45% was the best deformation rate for the microstructure of the material, which greatly improved the performance of the material.
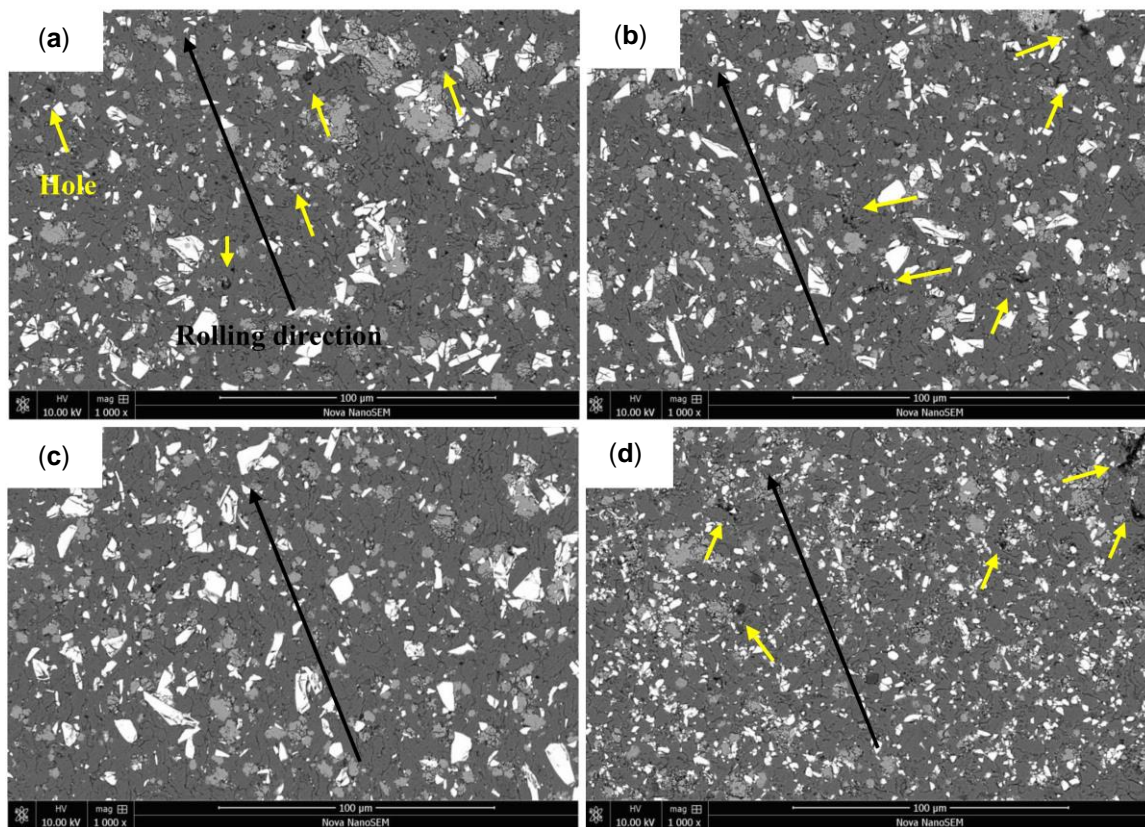

(**a**)15%; (**b**) 30%; (**c**) 45%; (**d**) 60% (along rolling direction).

Figure 3: SEM images of hot-rolled $Nd_2Fe_{14}B_p$/Al-5Co-0.4Sm at deformation rate.

Fig. (**4**) shows the typical phase and EDS analysis of $Nd_2Fe_{14}B_p$/Al-5Co-0.4Sm composites. In addition to the discovered phases $Nd_2Fe_{14}B$, Co, and $Nd_2(Fe, Co)_{14}B$ before adding Sm [8], a new phase Al_3Sm was found. The analysis showed that the electronegativities of Sm, Al, and Co were 1.17, 1.61, and 1.88, respectively. The electronegativity difference between Sm and Al was greater than that between Sm and Co, which was conducive to the preferential formation of the Al-Sm compound.

Fig. (**5**) shows the selected area scanning map of $Nd_2Fe_{14}B$/Al-5Co-0.4Sm composite with 45% deformation. Nd, Fe, and B were uniformly distributed, and the corresponding positions were the same, which confirmed the formation of the $Nd_2Fe_{14}B$ phase.
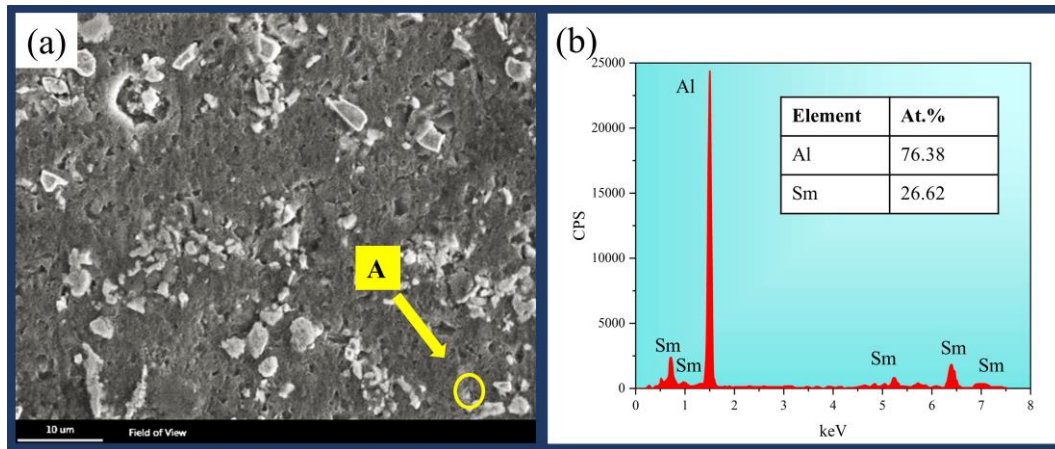
Figure 4: Typical phase and EDS analysis of Nd$_2$Fe$_{14}$B$_p$/Al-5Co-0.4Sm composites (**a**) typical phases; (**b**) EDS spectrum for phase A.
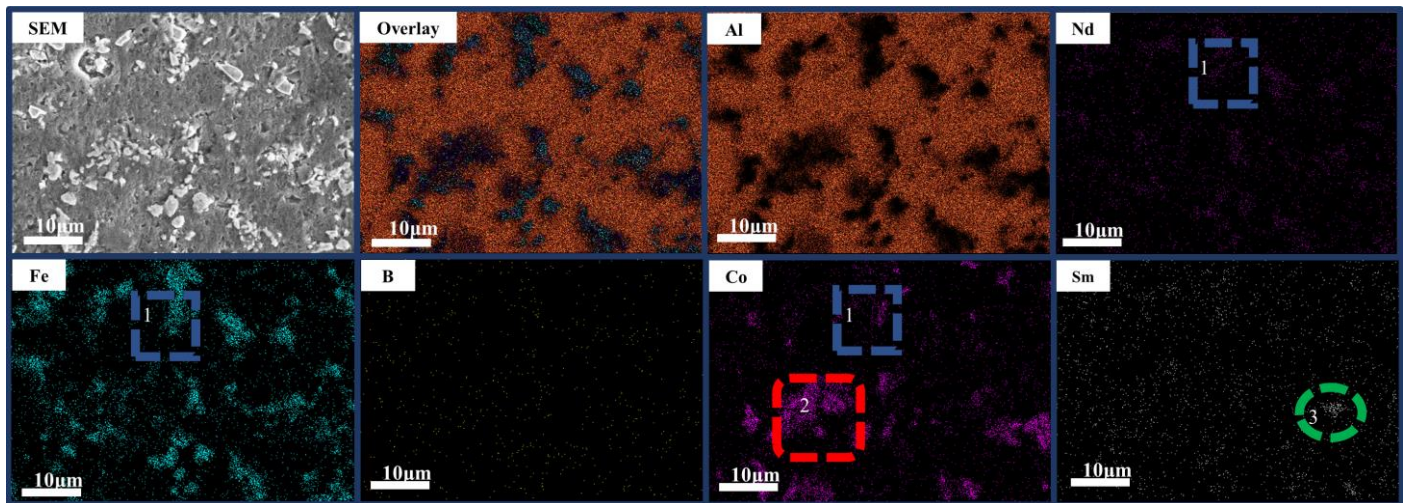
Figure 5: Selected surface scanning of Nd$_2$Fe$_{14}$B$_p$/Al-5Co-0.4Sm composites at a deformation rate of 45%.

There were three distribution behaviors of Co, as shown in marks 1-3. First, Co was attached to the surface of Nd$_2$Fe$_{14}$B particles as a surface active element to improve the wettability between Nd$_2$Fe$_{14}$B and Al matrix interface. Then it partially entered Nd$_2$Fe$_{14}$B and replaced Fe atoms, which changed the local structure and the magnetic properties of Nd$_2$Fe$_{14}$B, as shown in mark 1. Finally, it was dispersed in the matrix in the form of particles, playing a dispersion-strengthening role, as shown in mark 2.

From the distribution of Sm, part of Sm wrapped around the reinforcement particles greatly enhanced the interface bonding between the reinforcement (Nd$_2$Fe$_{14}$B) and the matrix (Al), making the distribution of Nd$_2$Fe$_{14}$B particles in the matrix more uniform and the structure of Nd$_2$Fe$_{14}$B/Al-5Co-0.4Sm composites more compact. As shown in mark 3, some Sm particles were dispersed in the matrix.

Fig. (**6**) shows a transmission electron microscope image of optimized hot-rolled Nd$_2$Fe$_{14}$B$_p$/Al-5Co-0.4Sm composites at a 45% deformation rate. As shown in Fig. (**6a**), many dislocation tangles were observed close to Nd$_2$Fe$_{14}$B particles. The observed dislocation tangles were attributed to the non-uniform deformation between the Nd$_2$Fe$_{14}$B particles and the aluminum matrix, which resulted in considerable distortion energy close to the particles. Consequently, a large number of dislocations in the area increased and entangled. Fig. (**6b**) shows high-resolution images of Nd$_2$Fe$_{14}$B and Al interfaces at mark (1) in Fig. (**6a**). Fig. (**6c**) shows the electron diffraction pattern at mark (2) in Fig. (**6b**). No other phases were formed at the interface, and only Al and Nd$_2$Fe$_{14}$B phases

existed. Fig. (**6d**) shows the inverse fast Fourier transform (IFFT) of mark (2) in (b). Severe lattice distortion occurred at the interface because of the mismatch between the reinforcing particles and the matrix caused by different crystal orientations, lattice spacing, and the mismatch of elastic modulus during rolling deformation. Fig. (**6e**) shows Co particles of different sizes around the interface and dislocation accumulation. Micron-sized Co particles were distributed in the aluminum matrix as a magnetic phase to strengthen the magnetic properties of the composite. The existence of nanoscale Co particles pinned dislocations and hindered the movement of dislocations, effectively improving the strength of composites.
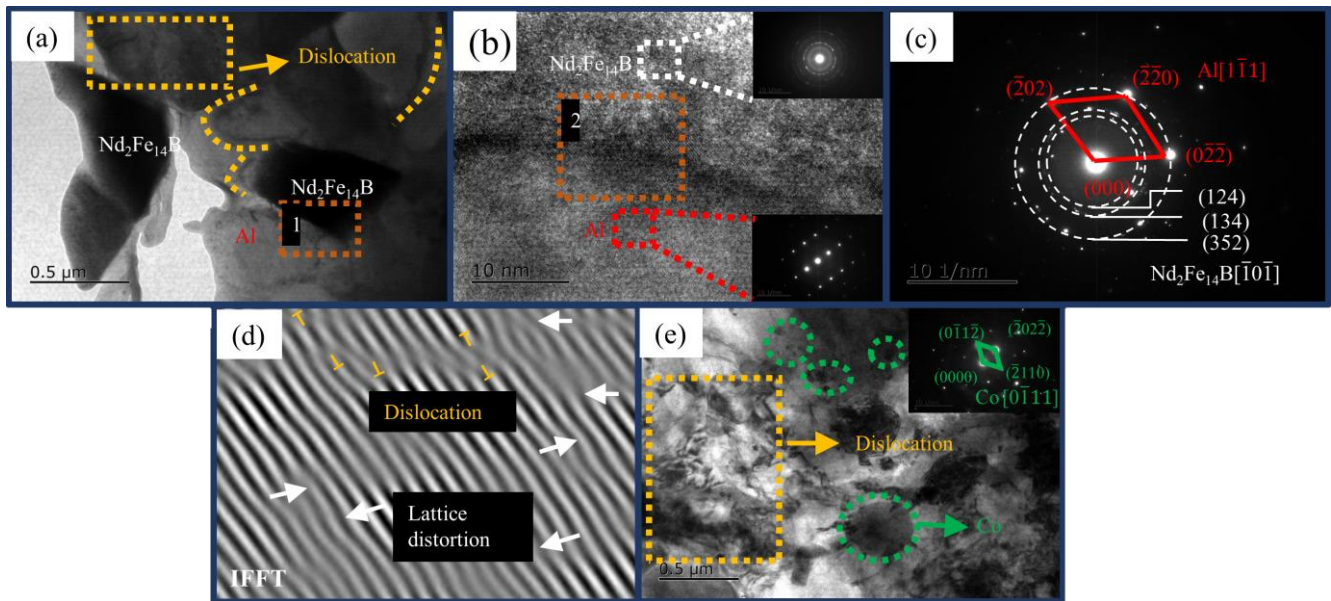
Figure 6: TEM images of hot-rolled $Nd_2Fe_{14}B_p$/Al-5Co-0.4Sm composites at a deformation rate of 45% (**a**) $Nd_2Fe_{14}B$ and dislocation; (**b**) High-resolution images of interfaces of mark (1) in (**a**); (**c**) Diffraction pattern of mark (2) in (**b**); (**d**) The inverse fast Fourier transform of mark (2) in (**b**); (**e**) Co phase.

3.2. Micromechanical Properties

Numerous finite element simulation analyses in the literature show that residual stress and plastic strain are concentrated close to the sharp angle of reinforced particles [26-28]. When the material is subjected to an external load, the sharp corners of the particles are prone to fracture. Therefore, to eliminate the influence of particle shape on dislocation formation and stress distribution around the interface, the smooth interface was selected for indentation experiments. The samples were tested at multiple points, and the average effect was taken. The corresponding test points were in the following order: aluminum matrix, external particles, and $Nd_2Fe_{14}B_p$/Al interface.

Fig. (**7a**) shows load-displacement (*P-h*) curves at the matrix of $Nd_2Fe_{14}B_p$/Al-5Co-0.4Sm composite materials with different deformations. With the increasing deformation rate, the indentation depth gradually decreased, indicating that the hardness of the matrix gradually increased. The numerical change trend of hardness and elastic modulus in Fig. (**7b**) indicates that when the deformation rate is 45%, the hardness and elastic modulus of the matrix is greatly improved compared with the unrolled sample. The hardness and elastic modulus of the matrix were 1.1 and 76 GPa, respectively, which increased by 142% and 24% compared with those of the unrolled sample, indicating that hot rolling can significantly improve the mechanical properties of the aluminum matrix. When the deformation rate increased to 60%, the hardness and elastic modulus of the composites decreased due to the recovery and recrystallization of the Al matrix.

Fig. (**7c**) shows the load-displacement (*P-h*) curves at the interface of $Nd_2Fe_{14}B_p$/Al-5Co-0.4Sm composite materials with different deformations. The indentation depth first decreased and then slightly increased as the deformation rate increased. Fig. (**7d**) shows the hardness and elastic modulus of the interface. The rolling

deformation greatly influenced the mechanical properties of the material interface. When the deformation rate increased in the following order 0%→15%→30%→45%, the hardness at the interface gradually increased, and the hardness was 3.6 GPa at a deformation rate of 45%, which increased by 117% compared with that of the non-rolled sample. At the same time, the elastic modulus fluctuated to a certain extent, reaching a maximum of 91GPa at a deformation rate of 45%. Compared with the non-rolled sample, the microhardness and elastic modulus at the interface of the rolled sample were improved, indicating that rolling strengthened the interface and contributed to the interface-strengthening effect of the material. It is indirectly confirmed that hot rolling can promote the bonding force and improve the interface strength between magnetic particles and the Al matrix to a certain extent. However, when the deformation was 60%, the hardness and elastic modulus of the reinforcement/matrix interface were reduced. When the rolling deformation rate was extremely high, the breakage of the $Nd_2Fe_{14}B$ particles reduced the bonding strength between the reinforcement and the matrix.
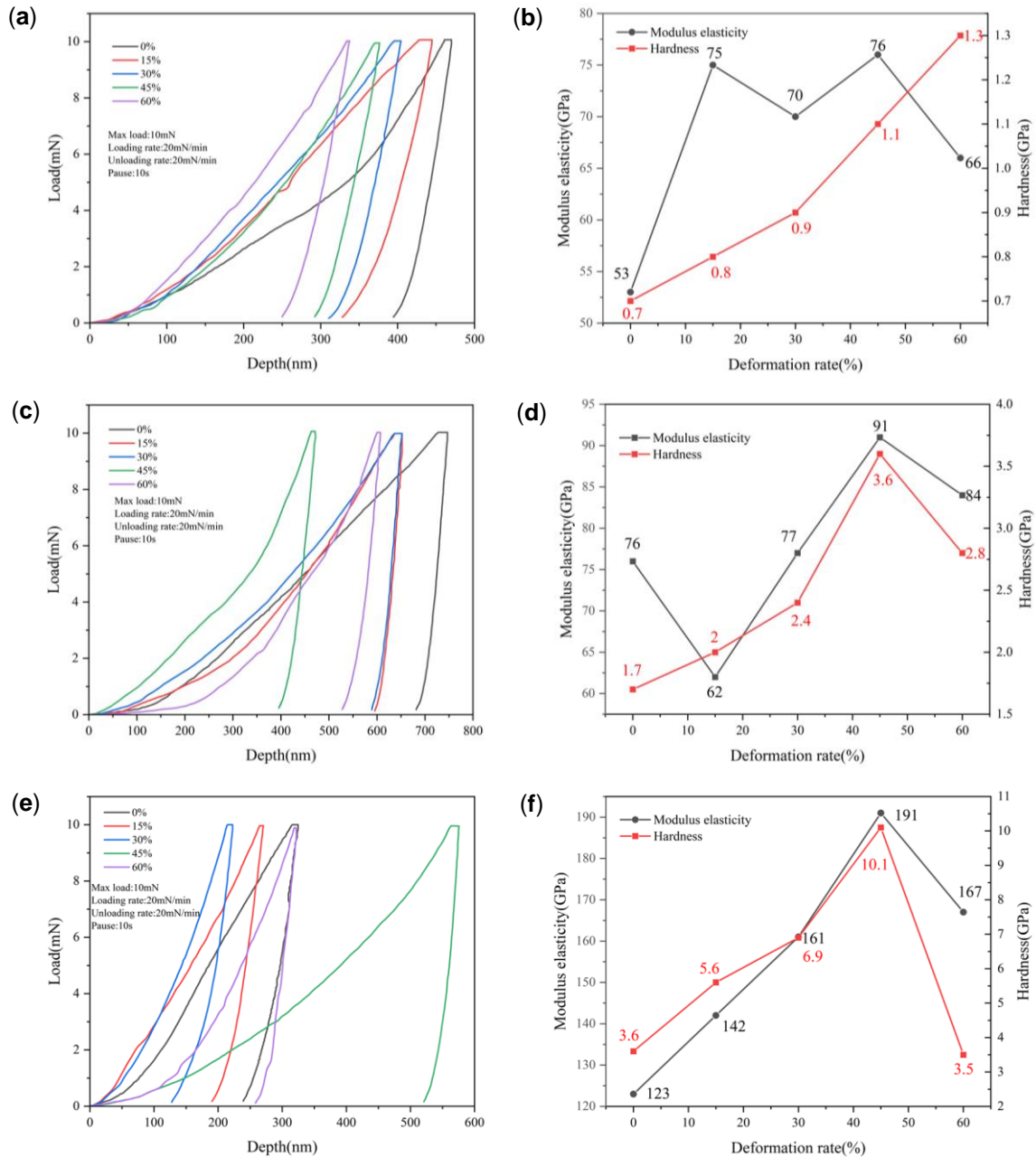
**Figure 7:** (**a**) Matrix nanoindentation load-displacement (*P-h*) curve of the composite material under different deformation rates; (**b**) hardness and elastic modulus at the matrix; (**c**) *P-h* curve at the interface; (**d**) the hardness and elastic modulus at the interface position; (**e**) the *P-h* curve at the enhanced phase; (**f**) the hardness and the elastic modulus at the enhanced phase.

Fig. (**7e**) and (**7f**) show the nanoindentation load-displacement (*P-h*) curves of hardness and elastic modulus at the reinforcement of $Nd_2Fe_{14}B_p$/Al-5Co-0.4Sm composite materials with different deformations. The hardness of $Nd_2Fe_{14}B$ increased when the deformation rate increased from 0 to 45%.in When the deformation was 45%, the maximum hardness and elastic moduli were 10.1 GPa and 191 GPa, respectively, contributing to the particle strengthening effect. When the deformation rate was 60%, the hardness and elastic modulus of particles were greatly decreased. The decrease of hardness and elastic modulus was due to the uncompact structure of $Nd_2Fe_{14}B$ particles. Therefore, the microhardness sharply decreased due to the crushing of $Nd_2Fe_{14}B$ under excessive pressure.

3.3. Tensile Properties and Fracture Morphology

Fig. (**8**) shows the effect of deformation rates on the mechanical properties of composites. When the deformation rate increased along 0→15%→30%→45%→60%, the tensile strengths gradually increased in the following order 141→148→152→161→and 173 MPa while the elongation decreased as follows: 8.9→8.6→7.2→6.5→5.7%. This phenomenon was consistent with the influence of deformation strengthening on mechanical properties.
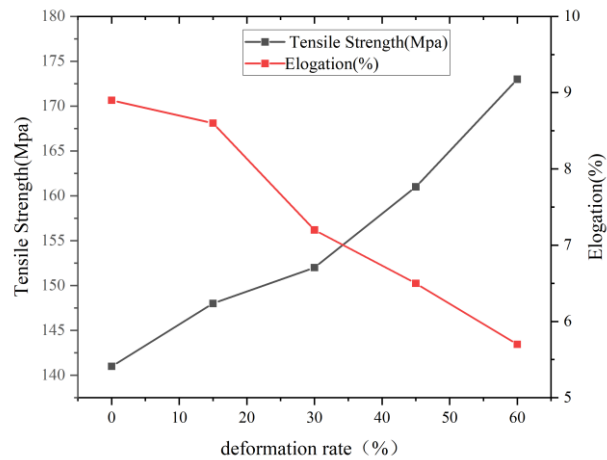

Figure 8: Tensile strength and elongation of hot-rolled $Nd_2Fe_{14}B_p$/Al-5Co-0.4Sm composites with different deformation rates.

Fig. (**9**) shows the fracture surface of the $Nd_2Fe_{14}B_p$/Al-5Co-0.4Sm composites with different deformation rates. The tensile fracture morphology of all hot-rolled composites exhibited the characteristics of brittle-ductile mixed fracture. There were numerous cleavage sections of $Nd_2Fe_{14}B$ particles or large-size $Nd_2Fe_{14}B$ particles, voids formed by particle exfoliation, tearing edges formed around the sections and voids, and small dimples formed by fracture of $Nd_2Fe_{14}B$ and Al matrix. As the deformation rate increased along 15%→30%→45%, the distribution uniformity of $Nd_2Fe_{14}B$ in the matrix was improved, and the connectivity between the particles and the Al matrix was greatly improved. Moreover, the interface bonding ability was enhanced, promoting the load transfer from the Al matrix to $Nd_2Fe_{14}B$ particles. When the deformation was 60%, the connectivity between the Al matrix and the $Nd_2Fe_{14}B$ became poor due to particle crushing, thus generating cracks. The cracks extended along the particle/matrix interface, resulting in the easy failure of composites. The fracture was in the form of a brittle fracture. The morphology of the fractured structure was consistent with the changing trend of mechanical properties.

Based on the microstructure evolution and mechanical properties of the hot-rolled $Nd_2Fe_{14}B_p$/Al-5Co-0.4Sm composites, the hot-rolled $Nd_2Fe_{14}B_p$/Al-5Co-0.4Sm composites with 45% deformation rate exhibited good strength and plasticity due to the following points:

1) Fine-grain strengthening during deformation. The grain structure is one of the main factors affecting the mechanical properties of composites [29, 30]. The refinement of the grains will increase the number of grain boundaries, which will hinder dislocations when they move to the grain boundaries, thus increasing the yield strength. The yield strength can be expressed using the Hall-Petch Equation [31],
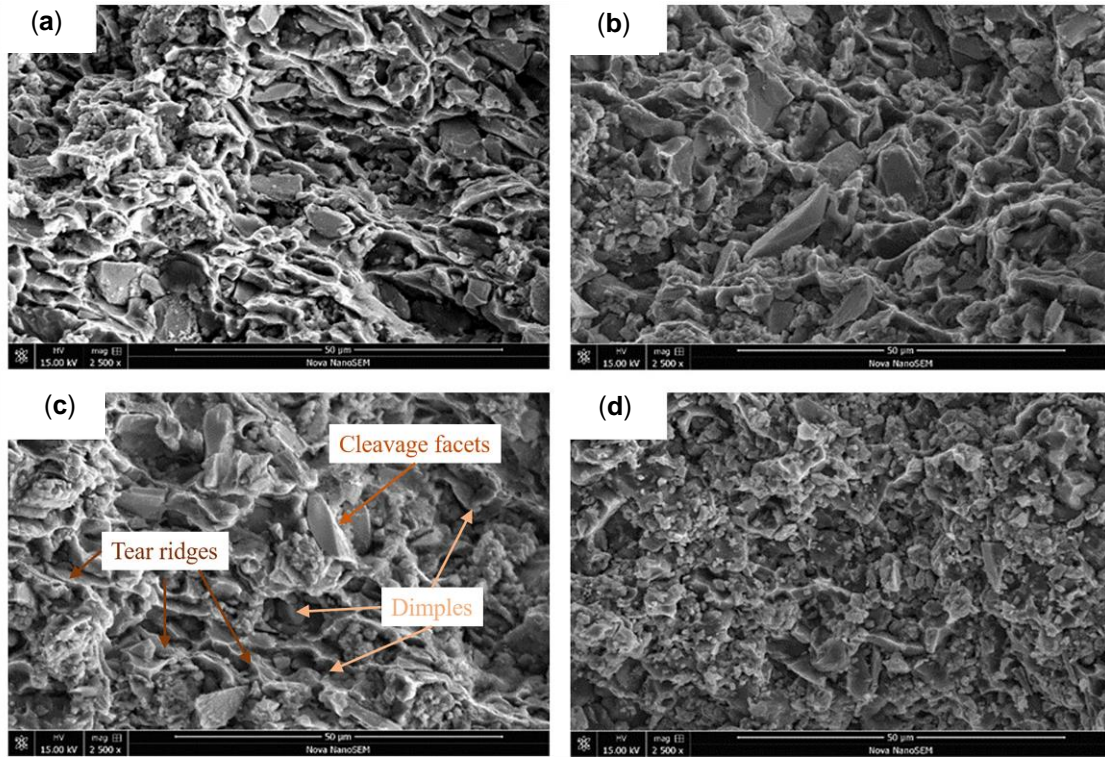
Figure 9: Tensile fracture morphology of hot-rolled $Nd_2Fe_{14}B_p$/Al-5Co-0.4Sm composites with different deformation rates (**a**) 15%; (**b**) 30%; (**d**) 45%; (**d**) 60%.

$$\Delta\sigma_1 = K(d^{-0.5} - d_0^{-0.5}) \tag{1}$$

where K = 0.07 is a constant, and d and d_0 are the grain sizes before and after hot rolling. The reduction of grain size improved the yield strength of the composite. Moreover, during the hot-rolling process, the uniformly distributed $Nd_2Fe_{14}B$ particles significantly limited the movement of the grain boundaries, which led to further refinement of the grains.

2) Dislocation enhancement. The dislocation strengthening effect of composites can be studied through the Taylor dislocation strengthening mechanism [33-36].

$$\Delta\sigma_2 = \beta Gb\sqrt{\rho} \tag{2}$$

where β = 1.25 is a constant; G = 25.4 GPa, which is the shear modulus of the Al matrix; b = 0.286 nm, which is the Burgers vector. Moreover, ρ is the dislocation density.

$$\rho = \frac{A\, \Delta\alpha\, \Delta T\, V_P}{bd\,(1-V_P)} \tag{3}$$

where A=10, which is a constant. $\Delta\alpha$ is the difference in thermal expansion coefficient between the aluminum matrix and the $Nd_2Fe_{14}B$ particles (the thermal expansion coefficient of Al is 26×10^{-6}/℃ and the thermal expansion coefficient of $Nd_2Fe_{14}B$ is 4×10^{-6}/℃), ΔT (480℃) is the maximum temperature difference during the preparation process, and V_p(7vol.%) is the volume fraction of $Nd_2Fe_{14}B$ particles.

Therefore, $\Delta\alpha$ is calculated as 12.36 MPa. As expressed in Equation (2), the greater the dislocation density, the greater the strength of the composites.

3) Orowan strengthening mechanism of $Nd_2Fe_{14}B$ [36-39]. Orowan strengthening is the strengthening effect caused by the hard particles that can hinder the passage of dislocations. The moving dislocations cannot pass

through the reinforcing particles but bypass the particles to leave dislocation loops. The smaller the spacing of the particle, the greater the curvature of the dislocation around the particle, showing a stronger obstacle effect and improving the yield strength of the material.

4. Conclusion

The following conclusions were drawn from this study:

1) When the deformation rate was 45%, the defects, such as internal pores, were reduced, and the grains of the aluminum matrix were elongated, indicating an enhanced orientation of the grains. Brittle $Nd_2Fe_{14}B$ particles were broken into fine particles under the action of rolling stress. As a result, the particles were more uniformly distributed, and the particle clusters significantly decreased. High-density dislocation tangles were observed around the particles.

2) The nanoindentation test results revealed that the hardness and elastic modulus of each micro-zone were in the following order: particle>interface>matrix. When the deformation rate was 45%, the nanoindentation hardness values at the particle, interface, and matrix were 10.1, 3.6, and 1.1 GPa, respectively, with the corresponding elastic modulus values of 191, 91, and 76 GPa.

3) From the perspective of tensile performance, as the deformation rate increased in the following order: 15%→30%→45%→60%, the tensile strength gradually increased, whereas the elongation gradually decreased. For the specimen at a deformation rate of 45%, the tensile strength and elongation were 161 MPa and 6.5%, respectively. The tensile strength ratio of the rolled sample increased by 14%.

Conflict of Interest

The authors declare that they have no known competing financial interests or personal relationships that may affect the work reported in this paper.

Funding

Acknowledgements

References

[1]   Tenaud P, Lemaire H, Vial F. Recent improvements in NdFeB sintered magnets. J Magn Magn Mater. 1991; 101(1-3): 328-32. https://doi.org/10.1016/0304-8853(91)90767-5

[2]   Sepehri-Amin H, Ohkubo T, Zaktonik M, Prosperi D, Afiuny P, Tudoret CO. Microstructure and magnetic properties of grain boundary modified recycled Nd-Fe-B sintered magnets. J Alloys Compd. 2017; 694: 175-84. https://doi.org/10.1016/j.jallcom.2016.09.305

[3]   Wang HM, Liu JQ, Li GR, Tang F, Yan YW, Gao LP. Effect of TiB2 content on microstructure and mechanical properties of (TiB2p+B4Cp)/Al composites fabricated by microwave sintering. J Mater Res Technol. 2021; 13: 1509-20. https://doi.org/10.1016/j.jmrt.2021.05.084

[4]   Wang HM, Ren WX, Li GR, Wen HR, Kai XZ. Microstructure and properties of FeCoNi1.5CrCu/2024Al composites prepared by microwave sintering. Mater Sci Eng. 2021; 801: 140406. https://doi.org/10.1016/j.mtcomm.2023.106022

[5]   Liu JQ, Wang HM, Li GR, Su WX, Zhang ZB, Zhou ZC, et al. Microstructure and improved plasticity of (FeCoNi1.5CrCu)p/Al composites subject to adjusted deep cryogenic treatment (DCT). J Alloys Compd. 2022; 895: 162690. https://doi.org/10.1016/j.jallcom.2021.162690

[6]   Gangil N, Siddiquee AN, Maheshwar S. Aluminium based in-situ composite fabrication through friction stir processing: A review. J Alloys Compd. 2017; 715: 91-104. https://doi.org/10.1016/j.jallcom.2017.04.309

[7]   Li GR, Xie ML, Wang HM, Xu T, Liu M. Microstructure and properties of Nd2Fe14B particles reinforced aluminum matrix composites synthesized by microwave sintering. Mater Res Express. 2019; 6: 026538. https://doi.org/ 10.1088/2053-1591/aaee07

[8]   Li GR, Chen JJ, Zhang D, Wang HM, Liu M, Tang F, et al. Microstructure and properties of the Nd2Fe14Bp/Al–Co composites fabricated via microwave sintering. J Mater Res Technol. 2021; 10: 34-50. https://doi.org/10.1016/j.jmrt.2020.11.084

[9]   Liu JQ, Wang HM, Huang ZH, Ma ZH, Li GR, Zhou PJ. Enhanced strength-ductility synergy of aging treated (FeCoNi1.5CrCu)p/2024Al composite. J Alloy Compd. 2022; 929:167372. https://doi.org/10.1016/j.jallcom.2022.167372

[10]   Camacho-Rios ML, Garay-Reyes CG, Lardizabal D, Estrada-Gue I, Perez-Bustamante R, Herrera-Pérez G, et al. Dispersion of graphite, Ceria, and nanohybrid Ceria-graphite in the 6063 aluminum alloy through powder metallurgy. Mater Chem Phys. 2022; 281: 125953. https://doi.org/10.1016/j.matchemphys.2022.125953

[11]   Manohar G, Pandey KM, Maity SR. Effect of variations in microwave processing temperatures on microstructural and mechanical properties of AA7075/SiC/graphite hybrid composite fabricated by powder metallurgy techniques. Silicon. 2022; 14: 7831-47. https://doi.org/10.1007/s12633-021-01554-x

[12]   Yang HY, Wang Z, Chen LY, Shu SL, Qiu F, Zhang LC, et al. Interface formation and bonding control in high-volume-fraction (TiC+TiB2)/Al composites and their roles in enhancing properties. Compos B Eng. 2021; 209: 108605. https://doi.org/10.1016/j.compositesb.2021.108605

[13]   Nie JF, Chen YY, Song L, Fan Y, Cao Y, Xie K, et al. Enhancing strength and ductility of Al-matrix composite via a dual-heterostructure strategy. Int J Plast. 2023; 171: 103825. https://doi.org/10.1016/j.ijplas.2023.103825

[14]   Wan B, Liu Y, Chen W, Lu T, Jin S, Xu X, et al. Effect of reinforcement types on the ball milling behavior and mechanical properties of 2024Al matrix composites. J Mater Res Technol. 2023; 23: 268-83. https://doi.org/10.1016/j.jmrt.2023.01.024

[15]   Wang HM, Li K, Li GR, Su WX, Chou SS, Wu TT, et al. Microstructure and properties of spinning deformed A356 alloy subject to the solution-DCT-aging multiplex heat treatment. J Mater Res Technol. 2023; 23: 5520-3. https://doi.org/10.1016/j.jmrt.2023.02.157

[16]   Zhou ZC, Gui GR, Wang HM, Zhou PJ, Dong K, Wei YM, et al. Effects of aging treatment on microstructure and mechanical properties of non-equiatomic high entropy alloy. Intermetallics. 2022; 153: 107799. https://doi.org/10.1016/j.intermet.2010.03.030

[17]   El-Sabbagh A, Soliman M, Taha M, Palkowski H. Hot rolling behaviour of stir-cast Al6061 and Al6082 alloys–SiC fine particulates reinforced composites. J Mater Process Technol. 2012; 212: 497-508. https://doi.org/10.1016/j.jmatprotec.2011.10.016

[18]   Lu TW, Scudino S, Chen WP, Wang P, Li D, Mao M, et al. The influence of nanocrystalline CoNiFeAl0.4Ti0.6Cr0.5 high entropy alloy particles addition on microstructure and mechanical properties of SiCp/7075Al composites. Mater Sci Eng. 2018; 726: 126-36. https://doi.org/10.1016/j.msea.2018.04.080

[19]   Zhang XZ, Chen TJ, Ma SM, Qin H, Ma J. Overcoming the strength-ductility trade-off of an aluminum matrix composite by novel core-shell structured reinforcing particulates. Compos B Eng. 2021; 206: 108541. https://doi.org/10.1016/j.compositesb.2020.108541

[20]   Feng ZH, Su H, Gao WL, Lu Z. Deformation microstructure and properties of SiCp/2024 composites cast by stirring during hot extrusion and rolling. Mater Rev. 2012; 26: 28-33. https://doi.org/ 10.3390/ma13122825

[21]   Ran T, Zhao Y, Kai X, Zhao Z, Ding R, Liang L, et al. Effects of hot rolling deformation on the microstructure and tensile properties of an in situ-generated ZrB2 nanoparticle-reinforced AA6111 composite. Mater Sci Eng. 2018; 732: 138-47. http://dx.doi.org/10.1016/j.msea.2018.06.107

[22]   Yu J, Lu Z, Xiong YC, Li GA, Feng ZH. Effect of intermediate thermomechanical treatment on microstructure and mechanical properties of 2A97 Al-Li alloy. Mater Sci Forum. 2019; 960: 70-7. https://doi.org/10.4028/www.scientific.net/MSF.960.70

[23]   Chen SJ, Oh HS, Gludovatz B, Kim SJ, Park ES, Zhang Z, et al. Real-time observations of TRIP-induced ultrahigh strain hardening in a dual-phase CrMnFeCoNi high-entropy alloy. Nat Commun. 2020; 11: 1-8. https://doi.org/ 10.1038/s41467-020-14641-1

[24]   Guo S, Chun NG, Lu J, Liu CT. Effect of valence electron concentration on stability of FCC or bcc phase in high entropy alloys. J Appl Phys. 2011; 109: 103505. https://doi.org/10.1063/1.3587228

[25]   L.J. Jing, Y. Pan, T. Lu, Pi J, Gu T. Nucleation potency prediction of LaB6 with E2EM model and its influence on microstructure and tensile properties of Al-7Si-0.3Mg alloy. Trans. Nonferrous Met Soc China. 2018; 28: 1687-94. https://doi.org/10.1016/S1003-6326(18)64812-5

[26]   Bolshakov A, Oliver WC, Pharr GM. Influences of stress on the measurement of mechanical properties using nanoindentation: Part II. Finite element simulations. J Mater Res. 1996; 11: 760-8. https://doi.org/10.1557/JMR.1996.0092

[27]   Shao JC, Xiao BL, Wang QZ, Ma ZY, Yang K. An enhanced FEM model for particle size dependent flow strengthening and interface damage in particle reinforced metal matrix composites. Compos Sci Technol. 2010; 71: 39-45. https://doi.org/10.1016/j.compscitech.2010.09.014

[28]   Spigarelli S, Cabibbo M, Evangelista E, Langdon TG. Creep properties of an Al-2024 composite reinforced with SiC particulates. Mater Sci Eng. 2002; 328: 39-47. https://doi.org/10.1016/S0921-5093(01)01698-7

[29]   Hirata H, Ogawa K. Metallurgical investigation and modelling of deterioration of creep rupture strength in heat affected zone of heat resistant ferritic steel. Mater High Temp. 2010; 27(3): 2192-226. https://doi.org/10.3184/096034010X1281977890495

[30]   Li CL, Choi SW, Oh JM, Hong JK, Yeom JT, Kang JH, et al. Bimodal grain structures and tensile properties of a biomedical Co–20Cr–15W–10Ni alloy with different pre-strains. Rare Met. 2021; 40: 20-30. https://doi.org/10.1007/s12598-020-01566-3

[31]   Mohsen K. Prediction of the mechanical properties of rods after cold forging and heat treatment. Int J Adv Manuf Technol. 2013; 69: 2071-9. https://doi.org/10.1007/s00170-013-5189-1

[32]   Jayalakshmi S, Gupta S, Sankaranarayanan S, Sahu S, Gupta M. Structural and mechanical properties of Ni60Nb40, amorphous alloy particle reinforced Al-based composites produced by microwave-assisted rapid sintering. Mater Sci Eng. 2013; 581: 119-27. https://doi.org/10.1016/j.msea.2013.05.072

[33]   Shang Z, Shen J, Wang L, Du Y, Xiong Y, Fu H. Investigations on the microstructure and room temperature fracture toughness of directionally solidified NiAl–Cr(Mo) eutectic alloy. Intermetallics. 2015; 57: 25-33. https://doi.org/10.1016/j.intermet.2014.09.012

[34]   Hossein-Zadeh M, Mirzaee O, Saidi P. Structural and mechanical characterization of Al-based composite reinforced with heat treated Al2O3 particles. Mater Des. 2013; 54: 245-50. https://doi.org/10.1016/j.matdes.2013.08.036

[35]   Suresh M, Kalsar R, More AM, Bisht A, Nayan N, Suwas S. Evolution of microstructure and texture in the third generation Al–Li alloy AA2195 during warm hybrid processing. J Alloys Compd. 2020; 855: 156750. https://doi.org/10.1016/j.jallcom.2020.156750

[36]   Zhang Z, Yang R, Guo Y, Chen G, Lei Y, Cheng Y, et al. Microstructural evolution and mechanical properties of ZrB2/6061Al nanocomposites processed by multi-pass friction stir processing. Mater Sci Eng. 2017; 689: 411-8. https://doi.org/10.1016/j.msea.2017.02.083

[37]   Zhao Z, Zhu H, Xie Z. In-situ TiC particles strengthen and ductilize Fe1.2MnNi0.8Cr high entropy alloy. Intermetallics. 2022; 140: 107398. https://doi.org/10.1016/j.intermet.2021.107398

[38]   Chen F, Chen Z, Mao F, Wang T, Cao Z. TiB2 reinforced aluminum based in situ composites fabricated by stir casting. Mater Sci Eng. 2015; 625: 357-68. https://doi.org/10.1016/j.msea.2014.12.033

[39]   Wu H, Huang S, Zhao C, Zhu H, Xie Z, Tu C, et al. Microstructures and mechanical properties of in-situ FeCrNiCu high entropy alloy matrix composites reinforced with NbC particles. Intermetallics. 2020; 127: 106983. https://doi.org/10.1016/j.intermet.2020.106983